

First principles study on the intrinsic resistivity of rectangular Ti_2B_2 and Mo_2B_2 Huiwen Zhang, Mingfeng Zhu,^{*} and Yisong Zheng[†]*Key Laboratory of Physics and Technology for Advanced Batteries (Ministry of Education),
College of Physics, Jilin University, Changchun 130012, China*

(Received 19 September 2023; revised 22 November 2023; accepted 8 December 2023; published 26 December 2023)

In the framework of semiclassical Boltzmann transport theory and by first principles calculations, we study the intrinsic resistivity (arising from the electron-phonon scattering) of two MBene materials: Ti_2B_2 and Mo_2B_2 . We find that the two kinds of MBenes are two-dimensional (2D) good conductors, with lower resistivity than other typical two-dimensional metals. For example, their intrinsic resistivity at room temperature is both significantly lower than the high-buckled plumbene and 2D Ti_3C_2 , noting that the latter possesses the maximal conductivity among MXene metals accessible so far. The impressive low resistivity of the two MBenes can be attributed to their sizable Fermi surface and relatively weaker electron-phonon (el-ph) interaction. What is more, we find the temperature dependence of the intrinsic resistivity of the two MBenes, i.e., the ρ - T relation, disagrees with the prediction of conventional Bloch-Grüneisen theory in both the low and high temperature limits. On one hand, the nontrivial umklapp scattering causes a notable deviation of the ρ - T relation of the two MBenes from the T^4 law, a general decay rate of 2D metals in the low temperature limit. On the other hand, on the high temperature side, the temperature dependence of the el-ph interaction's spectral function must be taken into account for describing correctly the ρ - T relation of actual materials with a sharply varying density of states of electrons around Fermi surfaces such as the case of the two MBenes, though it was often ignored in the relevant literature.

DOI: [10.1103/PhysRevB.108.245425](https://doi.org/10.1103/PhysRevB.108.245425)**I. INTRODUCTION**

Since graphene was exfoliated from graphite in 2004 [1], its unique electronic properties immediately attracted much attention. And tremendous interest in two-dimensional (2D) materials has been growing ever since. Recently, MBenes, an emerging class of 2D metals as the derivative of MXene, have gained significant attention due to their distinctive structural compositions and impressive electrical and mechanical characteristics [2]. Unlike conventional 2D transition metal borides, MBenes are a class of 2D transition metal borides with a layered sandwich structure obtained from the M - A - B phase, with the chemical formula $M_n\text{B}_{2n-2}$ ($n = 2, 3, 4$) [3]. Up to now, three rectangular $M_2\text{B}_2$ type MBenes have been successfully synthesized, namely Cr_2B_2 [4], Mo_2B_2 [5], and Ti_2B_2 [6]. Some MBenes have been proven to have high Li atom storage capacity, superior catalytic activity, and ultra-high Young's modulus [3]. Additionally, in some previous works it was mentioned that MBenes are good 2D conductors with high conductivity [7]. However, to our knowledge, there is no work as yet devoted to conducting a detailed investigation about the conductivity of any MBene materials, either experimentally or theoretically.

At and beyond room temperature, the conductivity or resistivity of metallic materials is dominated by electron-phonon (el-ph) scattering [8]. In contrast, other scattering

mechanisms, such as impurity and defect scatterings, contribute less significantly to the resistivity. In view of inevitable el-ph scattering even in a perfect lattice, the resistivity of metals arising from el-ph scattering is referred to as the intrinsic resistivity. In this study, within the semiclassical Boltzmann transport theory we perform first principles calculations to investigate the intrinsic resistivity of Ti_2B_2 and Mo_2B_2 , two kinds of nonmagnetic MBenes accessible thus far. In comparison to other typical 2D metals, our numerical results show that the intrinsic resistivity of Ti_2B_2 and Mo_2B_2 is not only much lower than some MXene materials with high conductivity, e.g., Ti_3C_2 and Ti_2N , but also lower than high-buckled (HB) plumbene, which is known for its excellent electrical conductivity. Our finding highlights the potential of MBenes as highly conductive 2D metallic materials.

The temperature dependence of the resistivity is an important characteristic of electric transport in metallic materials. According to the conventional Bloch-Grüneisen theory, the intrinsic resistivity of a metal varies linearly with temperature in the high temperature limit. However, in the low temperature limit, it decreases with temperature with a T^4 decay rate for 2D metals. Such a theoretical argument assumes a simple Fermi surface, but this is not the case for most actual metallic materials such as Ti_2B_2 and Mo_2B_2 . Therefore, a quantitative study on the temperature dependence of the intrinsic resistivity of these two MBenes in a wide temperature range is necessary. Our numerical results about the temperature dependence of the intrinsic resistivity, i.e., the ρ - T relations of the two kinds of MBenes, are inconsistent with the Bloch-Grüneisen theory in both the low and high temperature limits.

^{*}Corresponding author: mfzhu@jlu.edu.cn[†]Corresponding author: zhengys@jlu.edu.cn

On the low temperature side, we find that the violation of the T^4 law of the ρ - T relation is due to the nontrivial umklapp process of the el-ph scattering. More interestingly, on the high temperature side, the ρ - T relation of the two kinds of MBenes presents two separated linear regions, with the first one appearing at a much lower temperature than the Debye temperature. These findings go beyond the predictions of the Bloch-Grüneisen theory. By a detailed analysis, we find that the el-ph interaction spectral function independent of temperature is problematic, although it was frequently employed in the relevant literature. When the electronic density of states around the Fermi energy shows singularity to some extent, as the case of Ti_2B_2 and Mo_2B_2 , such a dubious spectral function might give an incorrect prediction about the ρ - T relation of actual metallic materials. Instead, the temperature dependence of the spectral function must be taken into account. Our finding is of key importance for understanding the temperature dependence of the intrinsic resistivity of actual metallic materials with complicated Fermi surfaces, and provides an essential complement to the Bloch-Grüneisen theory.

The remaining sections of this work are organized as follows. In Sec. II, we provide a brief description of the theoretical approach and computational details, including the Ziman resistivity formula for calculating the intrinsic resistivity and the technical details of the first principles calculations. The numerical results for the intrinsic resistivity of Ti_2B_2 and Mo_2B_2 are presented and discussed in Sec. III. Finally, the main results are summarized in Sec. IV.

II. THEORETICAL APPROACH AND COMPUTATIONAL METHODS

A. Ziman resistivity formula

The so-called Ziman resistivity formula [9], proposed first by Ziman based on a variational solution of the semiclassical Boltzmann transport equation, provides a theoretical approach for calculating the metallic resistivity subject to el-ph scattering. Subsequently, Allen extended it to more realistic situations, considering complex Fermi surfaces formed by multiple bands [10]. Thus, the Ziman resistivity formula enables the first principles calculations of the intrinsic resistivity of realistic metals, and it is often employed in much of the relevant literature. In response to a driving electric field in a specific orientation, say the x direction, the Ziman resistivity formula improved by Allen takes a form as

$$\rho_x = \frac{\pi}{e^2 \hbar N(E_f) \langle v_x^2 \rangle} \int d\Omega \alpha^2 F_T(\Omega) \mathcal{F}(k_B T / \Omega) \quad (1)$$

with the function

$$\mathcal{F}(k_B T / \Omega) = \frac{\Omega}{k_B T} \sinh^{-2} \left(\frac{\Omega}{2k_B T} \right) \quad (2)$$

and the el-ph interaction spectral function is defined as

$$\begin{aligned} \alpha^2 F_T(\Omega) &= \frac{1}{N_k N_q N(E_f)} \sum_{mnk\mathbf{q}} \frac{\delta(\Omega - \omega_{\nu\mathbf{q}})}{\omega_{\nu\mathbf{q}}} |G_{mn}^{\nu}(\mathbf{k}, \mathbf{q})|^2 \\ &\times \delta(E_{m\mathbf{k}+\mathbf{q}} - E_{n\mathbf{k}} - \hbar\omega_{\nu\mathbf{q}}) \\ &\times (f_{n\mathbf{k}} - f_{m\mathbf{k}+\mathbf{q}}) Q_{nk, m\mathbf{k}+\mathbf{q}}, \end{aligned} \quad (3)$$

where $Q_{nk, m\mathbf{k}+\mathbf{q}} = 1 - \frac{\mathbf{v}_{m\mathbf{k}+\mathbf{q}} \cdot \mathbf{v}_{n\mathbf{k}}}{|\mathbf{v}_{m\mathbf{k}+\mathbf{q}}| |\mathbf{v}_{n\mathbf{k}}|}$ is the large-angle scattering weight. In the above expressions, N_k and N_q represent the numbers of the electron wave vector \mathbf{k} and the phonon wave vector \mathbf{q} in the Brillouin zone (BZ) sampling, respectively. $N(E_f)$ stands for the electronic density of states (DOS) at the Fermi energy. $\omega_{\nu\mathbf{q}}$ denotes the frequency of the phonon state $|\nu\mathbf{q}\rangle$, where ν represents the indices of the phonon mode and \mathbf{q} is the phonon wave vector. $E_{n\mathbf{k}}$ and $E_{m\mathbf{k}+\mathbf{q}}$ correspond to the band energies of the electronic states $|n\mathbf{k}\rangle$ and $|m\mathbf{k}+\mathbf{q}\rangle$, respectively, where n and m denote the indices of the electron bands. $G_{mn}^{\nu}(\mathbf{k}, \mathbf{q})$ represents the el-ph interaction matrix element between an electronic initial state $|n\mathbf{k}\rangle$ and a final state $|m\mathbf{k}+\mathbf{q}\rangle$, resulting from the emission of a phonon state $|\nu-\mathbf{q}\rangle$ or absorption of a phonon state $|\nu\mathbf{q}\rangle$. $f_{n\mathbf{k}}$ and $f_{m\mathbf{k}+\mathbf{q}}$ are the Fermi-Dirac distribution functions of the individual electronic states. $\mathbf{v}_{n\mathbf{k}}$ and $\mathbf{v}_{m\mathbf{k}+\mathbf{q}}$ denote the electronic band velocities [9,11]. $\langle v_x^2 \rangle$ represents the squared average of the x component of electronic velocity on the Fermi surface,

$$\langle v_x^2 \rangle = \frac{\sum_{n\mathbf{k}} (\mathbf{v}_{n\mathbf{k}} \cdot \mathbf{e}_x)^2 \delta(E_{n\mathbf{k}} - E_f)}{\sum_{n\mathbf{k}} \delta(E_{n\mathbf{k}} - E_f)}. \quad (4)$$

What we would like to emphasize is that the spectral function given in Eq. (3) is temperature dependent. However, in Allen's original work, the spectral function is further approximated into a temperature-independent version which is expressed as

$$\begin{aligned} \alpha^2 \tilde{F}_T(\Omega) &= \frac{1}{N_k N_q N(E_f)} \sum_{mnk\mathbf{q}} \delta(\Omega - \omega_{\nu\mathbf{q}}) |G_{mn}^{\nu}(\mathbf{k}, \mathbf{q})|^2 \\ &\times \delta(E_{n\mathbf{k}} - E_f) \delta(E_{m\mathbf{k}+\mathbf{q}} - E_f) Q_{nk, m\mathbf{k}+\mathbf{q}}. \end{aligned} \quad (5)$$

In comparison with Eq. (3), we observe that two δ functions of electronic energy appear on the right side of Eq. (5). Therefore, in the literature it is often referred to as the el-ph interaction spectral function in the double δ -function approximation (DDFA). The DDFA restricts the initial and final electronic states joining the el-ph scattering exactly on the Fermi surface. In contrast, in the temperature dependent spectral function as shown in Eq. (3), those electronic states taking part in the el-ph scattering are allowed in an energy shell around the Fermi surface of a thickness of thermal excitation energy, which is referred to as the Fermi shell. The usage of the DDFA spectral function implies that temperature dependence of the intrinsic resistivity is solely determined by $\mathcal{F}(k_B T / \Omega)$ as defined by Eq. (2) which counts in only the thermal excitation of phonon number. The temperature smearing effect on the electronic Fermi surface is completely omitted. In fact, the DDFA, in spite of the wide usage in the previous literature, often brings about the incorrect prediction on the temperature dependence of intrinsic resistivity of some materials with complicated electronic structures. As seen below, the two kinds of MBenes under our consideration fall just into such a case.

For understanding the numerical results shown below, it is necessary to expose herein the approximations adopted for the evolution of the spectral function from Eq. (3) to Eq. (5). If we insert the identity $\int d\mathcal{E} \delta(\mathcal{E} - E_{n\mathbf{k}}) = 1$ into Eq. (3), we

then get

$$\begin{aligned}\alpha^2 F_T(\Omega) &= \int_{-\infty}^{\infty} d\varepsilon \frac{f(\varepsilon) - f(\varepsilon + \Omega)}{\Omega} I(\varepsilon, \Omega) \\ &\approx \int_{-\infty}^{\infty} d\varepsilon \left(-\frac{\partial f}{\partial \varepsilon} \right) I(\varepsilon, \Omega) \\ &\approx \alpha^2 \tilde{F}_T(\Omega) + \frac{\pi^2}{6} (k_B T)^2 \frac{\partial^2 I(\varepsilon, \Omega)}{\partial \varepsilon^2}\end{aligned}\quad (6)$$

with

$$\begin{aligned}I(\varepsilon, \Omega) &= \frac{1}{N_k N_q N(E_f)} \sum_{mnk} \delta(\Omega - \omega_{vq}) |\mathcal{G}_{mn}^v(\mathbf{k}, \mathbf{q})|^2 \\ &\times \delta(E_{m\mathbf{k}+\mathbf{q}} - E_{nk} - \hbar\omega_{vq}) \delta(\varepsilon - E_{nk}) Q_{nk, m\mathbf{k}+\mathbf{q}}.\end{aligned}\quad (7)$$

First, it is not difficult to find that the prerequisite from the second step to the third step of Eq. (6) is that the phonon energy, Ω , should be far smaller than the thermal excitation energy $k_B T$. Then, to reach the last result from the third step of Eq. (6), use has been made of the Sommerfeld expansion. Obviously, the Sommerfeld extension will become important as the temperature rises. What is more, to look at the second term in the Sommerfeld expansion of Eq. (6), one can readily find that even at a low temperature, when the second derivative of $I(\varepsilon, \Omega)$ gets nontrivial, the difference between the two kinds of spectral functions is not negligible. Such a case might occur when the electronic DOS in the Fermi shell shows singularity caused, for example, by the band edge. To sum up, the validity of the DDFA applied to the spectral function consists of the following two preconditions: the phonon energy to play the leading role for determining the intrinsic resistivity should be far smaller than $k_B T$. Then, the electronic DOS should be a slowly varying function in the Fermi shell.

When discussing in detail the numerical calculations of the intrinsic resistivity, there is a need to rewrite the expression of the resistivity given by Eq. (1) in a form as

$$\rho_x = \sum_{mnk} \sum_{vq} \rho_{mn}^v(\mathbf{k}, \mathbf{q}), \quad (8)$$

where

$$\begin{aligned}\rho_{mn}^v(\mathbf{k}, \mathbf{q}) &= \frac{\pi \beta}{e^2 \hbar N^2(E_f) \langle v_x^2 \rangle} \sinh^{-2} \left(\frac{\Omega}{2k_B T} \right) \\ &\times |\mathcal{G}_{mn}^v(\mathbf{k}, \mathbf{q})|^2 \delta(E_{m\mathbf{k}+\mathbf{q}} - E_{nk} - \hbar\omega_{vq}) \\ &\times (f_{nk} - f_{m\mathbf{k}+\mathbf{q}}) Q_{nk, m\mathbf{k}+\mathbf{q}}\end{aligned}\quad (9)$$

represents the contribution of the individual scattering process, i.e., $E_{nk} = E_{m\mathbf{k}+\mathbf{q}} + \omega_{vq}$, to the intrinsic resistivity. To clarify the contributions of the electronic or phonon states to the intrinsic resistivity, we can decompose Eq. (8) in different forms. First, we can define

$$\rho(\mathbf{q}) = \sum_{mn} \sum_{vk} \rho_{mn}^v(\mathbf{k}, \mathbf{q}); \quad (10)$$

$\rho(\mathbf{q})$ represents the contribution of the phonon wave vector \mathbf{q} to the intrinsic resistivity, i.e., \mathbf{q} -resolved resistivity. Based on

the above formula, we can define

$$\rho_{|\mathbf{q}|} = \sum_{q'} \rho(q') \delta(|\mathbf{q}| - |\mathbf{q}'|); \quad (11)$$

$\rho_{|\mathbf{q}|}$ represents the contribution of the phonons, with the length of the phonon wave vector equal to $|\mathbf{q}|$ to the intrinsic resistivity, i.e., $|\mathbf{q}|$ -resolved resistivity. Furthermore,

$$\rho^v = \sum_{\mathbf{q}} \rho^v(\mathbf{q}) = \sum_{\mathbf{q}} \sum_{mnk} \rho_{mn}^v(\mathbf{k}, \mathbf{q}); \quad (12)$$

$\rho^v(\mathbf{q})$ represents the contribution of the phonons with specific phonon state $|\nu\mathbf{q}\rangle$ to the intrinsic resistivity and ρ^v is the mode resolved intrinsic resistivity. Finally, we define

$$\rho(\mathbf{k}, \mathbf{k}') = \sum_{mn} \sum_{\nu} \rho_{mn}^v(\mathbf{k}, \mathbf{k} + \mathbf{q}), \quad (13)$$

which can be understood as the contribution of the electrons with the final state \mathbf{k}' to the intrinsic resistivity with the initial state fixed at \mathbf{k} .

B. Computational details

To obtain the intrinsic resistivity of Ti_2B_2 and Mo_2B_2 using the Ziman resistivity formula at the first principles levels, we first calculate the electronic and phonon states and el-ph interaction matrix elements of the metals. These calculations are performed within the frameworks of density functional theory (DFT) and density functional perturbation theory (DFPT) as implemented in the QUANTUM ESPRESSO software package [12]. We utilize a norm-conserving pseudopotential [13] to model the ionic potential and the Perdew-Burke-Ernzerhof (PBE) functional [14] within the generalized gradient approximation (GGA) for the exchange-correlation interaction. A 40 Ry cutoff energy is employed for the plane-wave basis set. To simulate the isolated two-dimensional system, a vacuum layer of 25 Å is added in the z direction to eliminate nonphysical interactions between periodic structures perpendicular to the plane direction. The two kinds of MBenes are composed of four atomic layers, though they belong to two-dimensional materials. To better describe the atomic interaction, especially among those atoms not belonging to the same or adjacent atomic layers, we take the vdW interaction into account, just as done in some previous works [15,16]. In so doing, the empirical DFT-D2 correction [17] is employed to describe the van der Waals interaction between the outermost nonbonding atoms. Our numerical results indicate that the vdW correction has only trivial impacts on the total energy and electronic band structure of the two MBenes. However, the optimized lattice parameters with vdW corrections are closer to the experimental values. Besides, the vdW correction can well eliminate the imaginary frequencies of the phonon dispersion of Ti_2B_2 and Mo_2B_2 near the Γ point. For Ti_2B_2 and Mo_2B_2 , we employ a $12 \times 12 \times 1$ \mathbf{k} mesh and a $4 \times 4 \times 1$ \mathbf{q} mesh sampled using the Monkhorst-Pack method [18] to cover the BZ. Finally, in order to achieve converged results with high precision of the intrinsic resistivity of the two kinds of MBenes, the knowledge of electronic and phonon dispersion, together with the el-ph interaction matrix elements

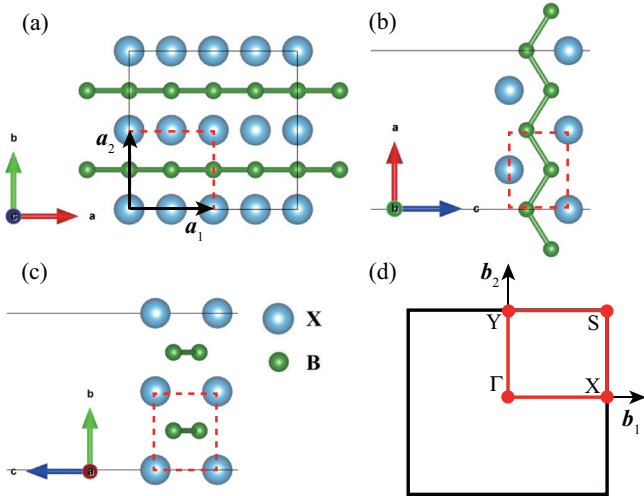


FIG. 1. (a) Top view, (b) side view 1, and (c) side view 2 of the lattice structure of rectangular M_2B_2 type MBenes. In (a), \mathbf{a}_1 and \mathbf{a}_2 represent the lattice vectors. The red dashed lines in (a), (b), and (c) indicate the unit cell. The blue balls represent the Ti or Mo atoms, and the green balls represent the B atoms. (d) Brillouin zone of the rectangular lattice with labeled high-symmetry points.

on ultrafine \mathbf{k} mesh and \mathbf{q} mesh, are required to calculate the intrinsic resistivity by means of the Ziman formula. But this implies a prohibitive computation cost if these quantities

are obtained directly on the level of DFT and DFPT. To circumvent such a prohibitive difficulty, we perform the calculation of intrinsic resistivity with a high precision by means of the Wannier interpolation technique. And such a kind of numerical calculation is implemented by the use of the EPW code [19]. Furthermore, in the calculations of the intrinsic resistivity, the Dirac- δ function is replaced by a Gaussian function with a specific width η . It can be seen below that with this approach we can obtain the intrinsic resistivity with the convergence precision smaller than 1%. It is indeed a very satisfactory numerical result.

III. RESULTS AND DISCUSSION

A. Crystal structure, electronic and phonon dispersion

The lattice structure and BZ of the rectangular M_2B_2 type MBenes are illustrated in Fig. 1. The relaxed lattice parameters are $\mathbf{a}_1 = 2.938 \text{ \AA}$, $\mathbf{a}_2 = 3.040 \text{ \AA}$ for Ti_2B_2 and $\mathbf{a}_1 = 3.021 \text{ \AA}$, $\mathbf{a}_2 = 3.030 \text{ \AA}$ for Mo_2B_2 . The electronic dispersions of Ti_2B_2 and Mo_2B_2 are presented in Figs. 2(a) and 2(c). The red solid lines represent the DFT results, while the blue dashed lines represent the results obtained through Wannier interpolation. Both calculations yield the same energy spectrum within an energy range of 1 eV around the Fermi energy, which is taken as the zero-energy reference. It is noteworthy that some band edges are very close to the Fermi level, as marked in Figs. 2(a) and 2(c). As shown in Figs. 2(b) and 2(d),

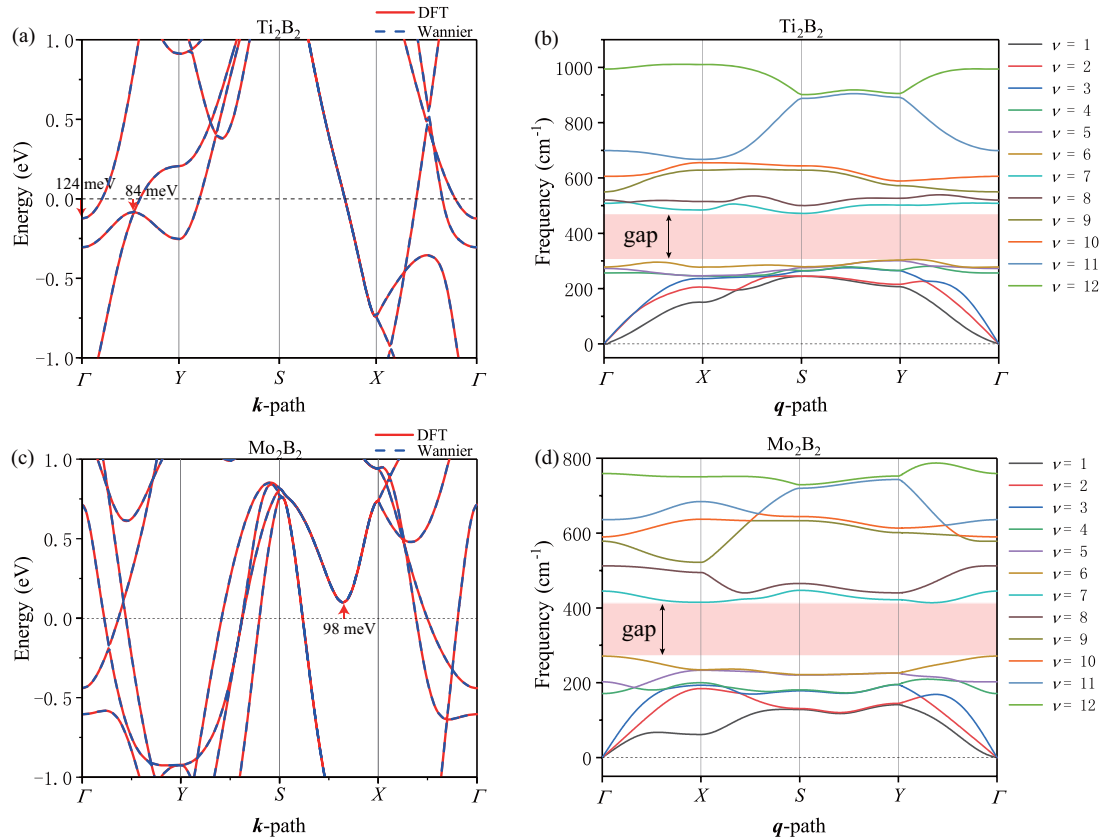


FIG. 2. (a) Electronic and (b) phonon dispersions of Ti_2B_2 along the high-symmetry path Γ -Y-S-X- Γ . (c) Electronic and (d) phonon dispersions of Mo_2B_2 along the high-symmetry path Γ -Y-S-X- Γ . The red solid lines in (a) and (c) represent the DFT results, while the blue dashed lines represent the results obtained through Wannier interpolation. The red shaded areas in (b) and (d) indicate the gap areas where low-frequency phonons are separated from high-frequency phonons.

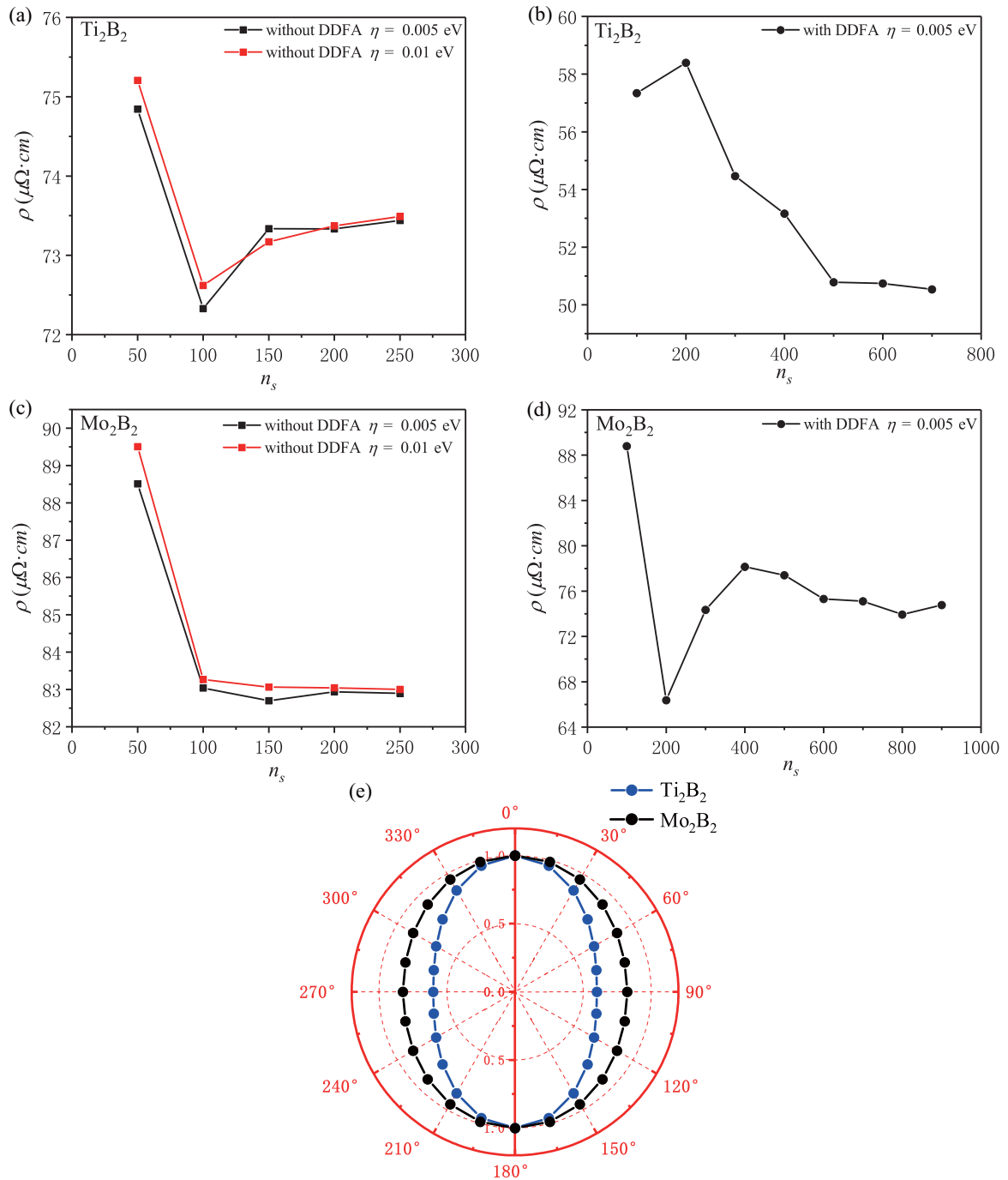


FIG. 3. The intrinsic resistivity of Ti_2B_2 with varying Gaussian broadening parameter η and $n_s \times n_s \times 1$ k and q mesh (a) without and (b) with DDFA. The intrinsic resistivity of Mo_2B_2 with varying Gaussian broadening parameter η and $n_s \times n_s \times 1$ k and q mesh (c) without and (d) with DDFA. (e) Resistivity $\rho(\theta)$ along different transport directions in the units of those along the x direction.

the phonon dispersions of Ti_2B_2 and Mo_2B_2 do not have any imaginary frequencies along the high symmetry lines. Twelve phonon modes exist in both Ti_2B_2 and Mo_2B_2 . The maximum phonon frequencies calculated for Ti_2B_2 and Mo_2B_2 are 1010 cm^{-1} and 787 cm^{-1} , respectively, which can be regarded as the Debye frequency. The corresponding Debye temperatures are $T_D = 1453 \text{ K}$ for Ti_2B_2 and $T_D = 1132 \text{ K}$ for Mo_2B_2 . Moreover, it is evident that the entire phonon dispersion can be divided into two regions, the low-frequency

phonon (LP) modes ($\nu = 1-6$) and the high-frequency phonon (HP) modes ($\nu = 7-12$).

B. Intrinsic resistivity of Ti_2B_2 and Mo_2B_2

With the formulation presented above, we are now ready to study numerically the intrinsic resistivity of the two kinds of MBenes. First of all, it is essential to conduct a convergence test on the calculated intrinsic resistivity with

TABLE I. Intrinsic resistivity values of graphene, HB-plumbene, Ti_3C_2 , Ti_2N , Ti_2C , Nb_4C_3 , Ti_2B_2 , and Mo_2B_2 at room temperature (300 K). The resistivity of graphene calculated in the case of weaker doping. (The electron doping concentration is $4 \times 10^{11} \text{ cm}^{-2}$; i.e., the Fermi energy level is shifted by 0.12 eV. The unit cell thickness of the perpendicular graphene sheet is taken to be 20 Å.)

2D material	Intrinsic resistivity ($\mu\Omega \text{ cm}$)
Graphene	2 [20] (cal.)
HB-plumbene	74 [21] (cal.)
Ti_3C_2	154 [22] (exp.)
Ti_2N	163 [23] (cal.)
Ti_2C	6 800 000 [24] (exp.)
Nb_4C_3	460 000 [25] (exp.)
$\text{Ti}_2\text{B}_2 \rho_x (\rho_y)$	73.4 (44.1) (our work)
$\text{Mo}_2\text{B}_2 \rho_x (\rho_y)$	83.0 (68.3) (our work)

regard to the density of \mathbf{k} and \mathbf{q} mesh as well as Gaussian spreading parameter η . As shown in Fig. 3(a), if the spectral function without the DDFA is used, the numerical result of the intrinsic resistivity converges when the \mathbf{k} and \mathbf{q} mesh both amount to a density of $200 \times 200 \times 1$, together with the Gaussian spreading parameter $\eta = 0.005 \text{ eV}$. In contrast, as illustrated in Fig. 3(b), when the DDFA is adopted to approximate the spectral function, it requires much denser grids for BZ sampling, i.e., $600 \times 600 \times 1$ \mathbf{k} and \mathbf{q} mesh. In Figs. 3(c) and 3(d), it is the similar case with the convergence test of the calculated intrinsic resistivity of Mo_2B_2 . In all cases, the relative errors of the obtained intrinsic resistivity are less than 1%. These convergence tests ensure the accuracy and reliability of our calculations. In addition, the intrinsic resistivities of Ti_2B_2 and Mo_2B_2 both show weak anisotropy with the highest resistivity along the x direction and the lowest one along the y direction as shown in Fig. 3(e). Of course, as seen from Eq. (1), the anisotropy of the intrinsic resistivity arises from the Fermi surface average of the squared velocity component along the transport direction which varies with the direction of the driving electric field if the Fermi surface deviates from an ideal circle for any 2D material.

With the obtained high-precision intrinsic resistivity of the MBenes, it is significant to assess their electric transport ability in comparison with those of other typical 2D materials currently available. The intrinsic resistivities of Ti_2B_2 and Mo_2B_2 , as well as those of several typical 2D metallic materials, are presented in Table I. As displayed in Table I, the intrinsic resistivities of Ti_2B_2 and Mo_2B_2 are only an order of magnitude higher than that of graphene with appropriate carrier doping and lower than those of most 2D metallic materials. Specifically, the resistivities of both Ti_2B_2 and Mo_2B_2 along the y direction are lower than that of isotropic HB-plumbene, which has the lowest intrinsic resistivity in Table I except for graphene. More interestingly, as derivatives of MXene, Ti_2B_2 and Mo_2B_2 exhibit lower resistivity than Ti_3C_2 , which possesses the lowest resistivity at room temperature among MXenes available thus far. This suggests that the two kinds of MBenes, as the 2D metals, are 2D good conductors. To further identify the reasons for the low resistivity of MBenes, we conduct a comparative analysis below. For simplicity and to obtain the upper limit of the intrinsic

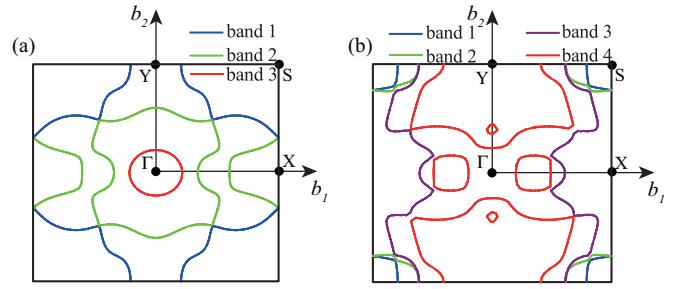


FIG. 4. The Fermi surfaces of (a) Ti_2B_2 and (b) Mo_2B_2 . Different colors indicate distinct bands crossing the Fermi surface, and \mathbf{b}_1 and \mathbf{b}_2 represent the reciprocal lattice vectors.

resistivity, we focus solely on ρ_x in subsequent discussions. According to the Ziman formula, the intrinsic resistivity is inversely proportional to $N(E_f)$ and $\langle v_x^2 \rangle$ at Fermi surface. Besides, it is also proportional to the strength of el-ph scattering, which is measured by the integral of the product of the $\alpha^2 F_T(\Omega)$ and the $\mathcal{F}(k_B T/\Omega)$ function, as given in Eq. (1). For simplicity, we denote such an integral as \mathcal{W} . Therefore, our comparative analysis will focus on the following three factors: $N(E_f)$, $\langle v_x^2 \rangle$, and \mathcal{W} . Table II presents the values of $N(E_f)$, $\langle v_x^2 \rangle$, and \mathcal{W} for graphene, Ti_2B_2 , Mo_2B_2 , HB-plumbene, and Ti_2N . Compared with graphene, MBenes have larger DOS at Fermi level, which is consistent with the plots of Fermi surfaces shown in Fig. 4. This means that MBenes host more carriers to take part in the electric transport. However, weakly doped graphene has a much smaller Fermi surface around the Dirac point, allowing only phonons with specific wavelengths to participate in el-ph scattering. Besides, the backscattering is lacking due to the chiral electron characteristic of graphene. Consequently, the strength of the el-ph scattering is very weak, resulting in a small \mathcal{W} in graphene. Although the el-ph scattering is much stronger than that of graphene, as shown in Table II, it is not strong compared to other 2D materials. Considering these three factors that determine the intrinsic resistivity, we conclude that it is the weaker strength of el-ph interactions and a larger Fermi surface that lead to the relatively low resistivity in MBenes.

C. Temperature dependence of intrinsic resistivity

The temperature dependence of the resistivity is an important electric transport characteristic of metallic materials. According to the conventional Bloch-Grüneisen theory, the intrinsic resistivity of a metal depends on temperature linearly in the high temperature limit. For metals, the starting temperature of such a linear ρ - T relationship often exceeds the Debye temperature above which all phonon modes are fully thermally excited and consequently the phonon number is proportional to the temperature. Because the el-ph scattering rate has a linear relation with the phonon number, it is a straightforward result that the intrinsic resistivity of metal exhibits a linear temperature dependence in the high temperature limit. On the other hand, at the low temperature limit, if the umklapp el-ph scattering is trivial, the intrinsic resistivity of a 2D metal shows a T^4 decay rate as the

TABLE II. The numerical values of three factors $N(E_f)$, $\langle v_x^2 \rangle$, and \mathcal{W} in different materials.

Factors	Materials				
	Graphene	Ti ₂ B ₂	Mo ₂ B ₂	HB-plumbene	Ti ₂ N
$N(E_f)$ (eV ⁻¹)	0.007	1.585	1.564	0.754	8.925
$\langle v_x^2 \rangle$ ($\times 10^{12}$ m ² s ⁻²)	4.571	0.551	1.377	8.656	0.173
\mathcal{W} ($\times 10^{-24}$ $\mu\Omega$ m ³ A ²)	0.341	343.552	958.440	2589.565	1347.563

temperature approaches zero. But all these theoretical predictions are limited within a simple Fermi surface. However, as seen from Fig. 4, the two kinds of MBenes both possess complicated Fermi surfaces. Therefore, it is necessary for us to study in detail the temperature dependence of the intrinsic resistivity of MBenes. The calculated ρ - T relationships of Ti₂B₂ and Mo₂B₂ at a much lower temperature region are presented in Figs. 5(a) and 5(b). By fitting the ρ - T curves, it is evident that Ti₂B₂ exhibits a T^3 dependence, while Mo₂B₂ exhibits a $T^{2.34}$ dependence, both breaking the T^4 law. Moreover, at higher temperature regions,

the intrinsic resistivity versus temperature of Ti₂B₂ and Mo₂B₂ calculated with and without DDFA is presented in Figs. 5(c) and 5(d). The intrinsic resistivity of Ti₂B₂ and Mo₂B₂ calculated without DDFA exhibits two separate regions of linear temperature dependence. For Ti₂B₂, the first one occurs within 100–600 K, which is lower than the Debye temperature, while the onset temperature of the second linear temperature dependence region is about 1400 K. Similarly, for Mo₂B₂, one occurs below the Debye temperature (100–900 K) and another above it ($T > 1600$ K). The appearance of the first linear temperature dependence region is

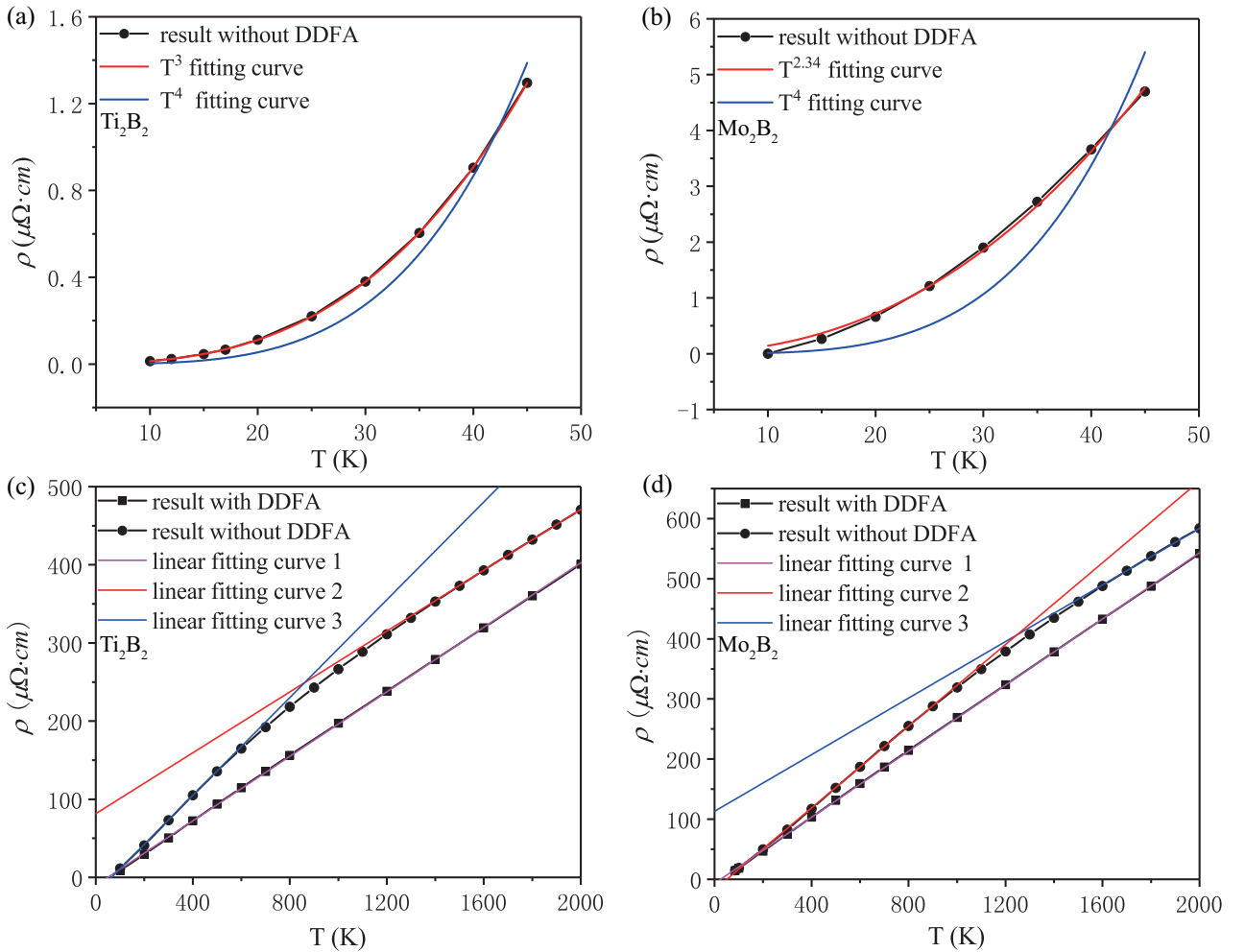


FIG. 5. Intrinsic resistivity of (a) Ti₂B₂ and (b) Mo₂B₂ calculated by $\alpha^2 F_T$ vs temperature T within 10–45 K. In (a), the T^4 fitting curve (blue solid line) and T^3 fitting curve (red solid line) are plotted for comparison. In (b), the T^4 fitting curve (blue solid line) and $T^{2.34}$ fitting curve (red solid line) are plotted for comparison. Intrinsic resistivity of (c) Ti₂B₂ and (d) Mo₂B₂ calculated by $\alpha^2 F_T$ (circle point-line) and $\alpha^2 \tilde{F}_T$ (rectangular point-line) vs temperature T within 100–2000 K, with the linear fitting curves plotted for comparison.

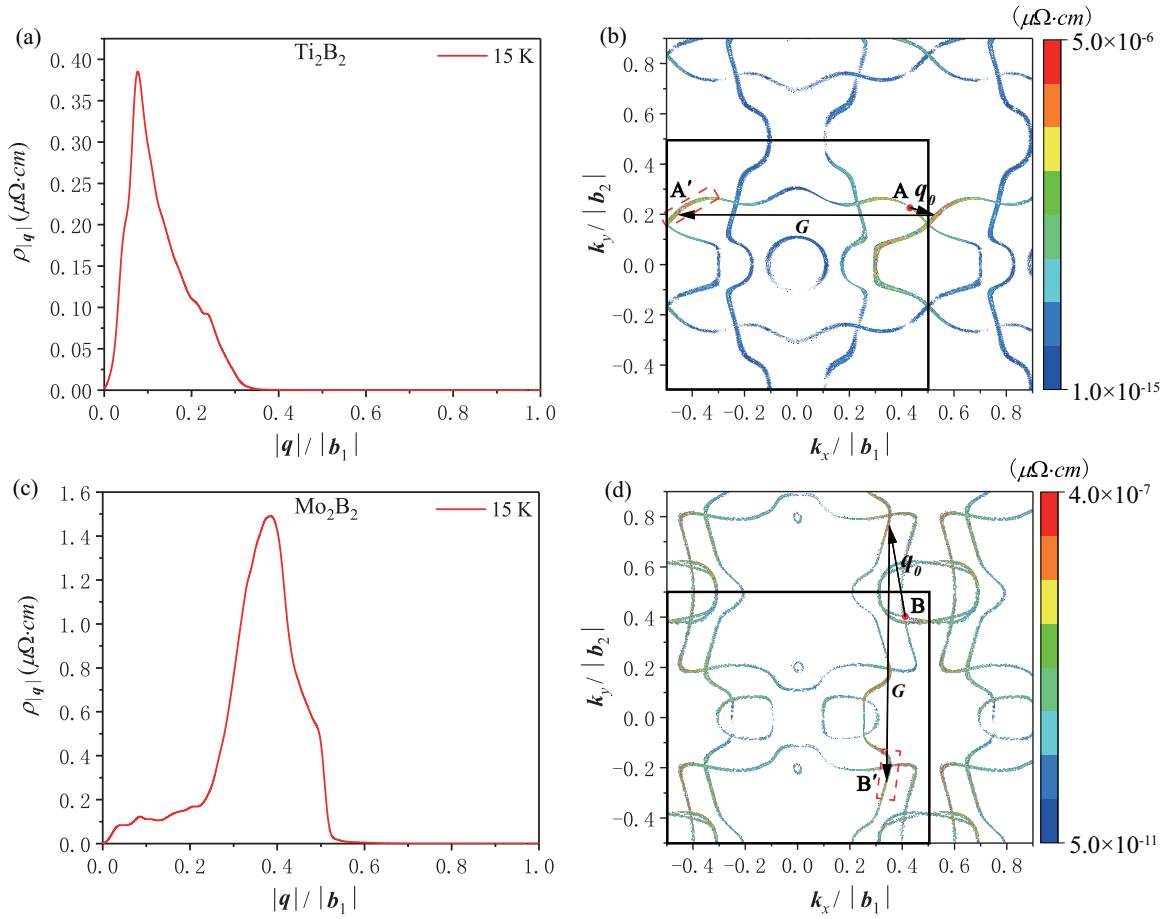


FIG. 6. The plot shows the $|\mathbf{q}|$ -resolved resistivity, $\rho_{|\mathbf{q}|}$, of (a) Ti_2B_2 and (c) Mo_2B_2 at 15 K, with peaks observed at $0.08|b_1|$ and $0.38|b_1|$, respectively. The final-state \mathbf{k}' -resolved resistivity of (b) Ti_2B_2 and (d) Mo_2B_2 at 15 K, where the first Brillouin zone (1BZ) is indicated by the black solid lines. In (b) and (d), points A and B are selected initial states, and points A' and B' denote the initial states that contribute heavily to the resistivity, respectively.

at odds with the prediction of the Bloch-Grüneisen theory since the onset temperature (about 100 K) is much lower than the Debye temperature. However, as shown in Figs. 5(c) and 5(d), the ρ - T curves of Ti_2B_2 and Mo_2B_2 calculated with DDFA are always linear in the temperature range of 100–2000 K.

At the low temperature limit, the possible reason for the breakdown of the T^4 law is the nontrivial umklapp el-ph scattering [26–28] which is disregarded in the Bloch-Grüneisen theory. Such a scattering follows the conservation of lattice momentum, $\mathbf{k}' = \mathbf{k} + \mathbf{q} + \mathbf{G}$, with a nonzero reciprocal lattice vector \mathbf{G} . It often relates to the large-angle scattering which leads to significant change in the velocity of electrons [11]. Consequently, it could play the key role in breaking the T^4 law. In Fig. 6, we present the $|\mathbf{q}|$ -resolved resistivity and final-state \mathbf{k}' -resolved resistivity for Ti_2B_2 and Mo_2B_2 . As shown by Eq. (13), the \mathbf{k}' -resolved resistivity is determined by the difference between \mathbf{k} and \mathbf{k}' . Thus, with a given \mathbf{k} , $\rho(\mathbf{k}, \mathbf{k}')$ as a function \mathbf{k}' does not obey the complete symmetry of the Fermi surface. As illustrated in Fig. 6(a), for Ti_2B_2 , the $|\mathbf{q}|$ -resolved resistivity peaks at $|\mathbf{q}| = 0.08|b_1|$. It indicates

that the resistivity is dominated by long-wavelength phonons at low temperatures such as 15 K. Therefore, when the initial state \mathbf{k} is set at point A, the final states \mathbf{k}' , which significantly contribute to the resistivity, are mainly distributed near point A, as illustrated in Fig. 6(b). In addition, we can see that there are some final states \mathbf{k}' in the upper left region of the first Brillouin zone (1BZ) that have a nontrivial contribution to the resistivity, as indicated by the red dashed bordered rectangle in Fig. 6(b). As the involved phonons in el-ph scattering are mainly the long-wavelength ones, such a scattering is mostly implemented via an umklapp process as labeled in Fig. 6(b). From the numerical results shown in Figs. 6(c) and 6(d), we can infer that in Mo_2B_2 , the umklapp scattering is equally important. In addition, it should be noticed that the occurrence of the umklapp process is favored by the large Fermi surface of both types of MBenes. In the high temperature region, according to conventional transport theory, once the temperature exceeds the Debye temperature largely, full thermal excitation of all phonon modes is realized. Then, the ρ - T relation begins to show a linear behavior. However, for the two kinds of MBenes, as observed in Figs. 5(c) and 5(d), such

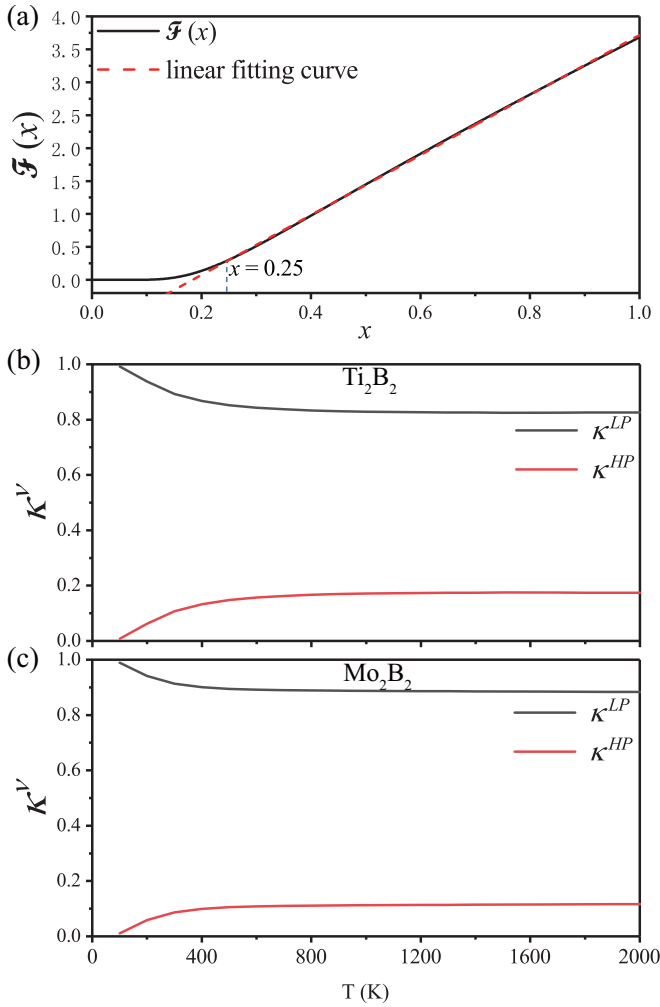


FIG. 7. (a) The plot of the function $\mathcal{F}(T/T_0)$. Percentage contributions of LP (solid black line) and HP (solid red line) of (b) Ti_2B_2 and (c) Mo_2B_2 to the intrinsic resistivity at different temperatures.

a simple argument cannot well explain the appearance of the first linear ρ - T region with an onset temperature much lower than Debye temperature. In fact, such a complicated ρ - T relation of MBenes is tightly associated with the nontrivial temperature dependence of the el-ph interaction spectral function. Within the DDFA, the temperature dependence of the el-ph interaction spectral function is completely disregarded. Therefore, the temperature dependence of the intrinsic resistivity is determined only by the $\mathcal{F}(x)$ function defined by Eq. (2). As shown in Fig. 7(a), we find that $\mathcal{F}(x)$ begins to show a linear profile when $x > 0.25$. Accordingly, from Eq. (1) we can infer that when $T > 0.25T_0$, the function $\mathcal{F}(T/T_0)$ triggers the linear ρ - T relation, where T_0 refers to a characteristic temperature corresponding to the full thermal excitation of the phonon mode which has a leading contribution to the intrinsic resistivity. Even though we makes a conservative estimate as $T_0 = T_D$, such an argument indicates that the linear ρ - T relation starts at a temperature lower than the Debye temperature. By defining $\kappa^{LP} = \sum_{\nu=1}^6 \rho_{\nu}^v / \rho_x$

and $\kappa^{HP} = \sum_{\nu=7}^{12} \rho_{\nu}^v / \rho_x$, which stand for the respective percentages of the contributions of LP and HP to the intrinsic resistivity, we find that the LP contributes more than 80% of the total resistivity for both Ti_2B_2 and Mo_2B_2 in the whole temperature range, as illustrated in Figs. 7(b) and 7(c). Therefore, we can identify $T_0 \approx 450$ K for Ti_2B_2 and $T_0 \approx 400$ K for Mo_2B_2 , namely, the characteristic temperatures corresponding to the cutoff frequencies of the LP of these two materials. Consequently, the estimated onset temperatures of the linear ρ - T relationships for Ti_2B_2 and Mo_2B_2 are about 100 K, which agrees well with the onset temperatures of the linear ρ - T curve of DDFA shown in Figs. 5(c) and 5(d).

From the band structures of MBenes shown in Figs. 2(a) and 2(c), we can see that some band edges occur near the Fermi levels of MBenes. With the rise of temperature, the Fermi shell broadens. Thus, these band edges enter the Fermi shell, giving rise to the drastic variation of the DOS around energy. In such a situation, as seen from Eq. (6), the Sommerfeld correction term becomes important in affecting the spectral function. In other words, the DDFA becomes invalid and the temperature dependence of the spectral function gets relevant to the ρ - T relation. Due to such a reason, the intrinsic resistivity calculated with the temperature dependent spectral function as shown in Eq. (3) deviates from the linear temperature dependence gradually with the increase of temperature.

IV. CONCLUSION

In this investigation, we delved into the intrinsic resistivity characteristics of two synthesized MBenes, namely Ti_2B_2 and Mo_2B_2 , utilizing the Ziman resistivity formula within the frameworks of DFT and DFPT. Through a comprehensive comparison encompassing the intrinsic resistivity of various 2D materials, we find that the intrinsic resistivities of Ti_2B_2 and Mo_2B_2 are positioned merely one order of magnitude above that of graphene, while aligning with the same order of magnitude as the exceptional conductivity showcased by materials such as HB-plumbene. This observation unequivocally underscores the potential of MBenes as a class of highly conductive 2D metals. Additionally, as we dissect the triad of factors governing the magnitude of intrinsic resistivity, it becomes evident that MBenes not only possess weaker el-ph interactions but also feature significantly larger Fermi surfaces, thereby accommodating a substantial number of carriers engaged in the process of transport.

Moreover, we observed that the ρ - T relationships of Ti_2B_2 and Mo_2B_2 do not conform to the prediction of the Bloch-Grüneisen theory in either the high or low temperature regions. At low temperature, umklapp scattering plays the leading role in breaking the T^4 law for 2D metals. At higher temperature, we find that the band edges near the Fermi level play important roles in breaking the linear relationship between resistivity and temperature predicted by DDFA. Therefore, it is essential to use the temperature dependent spectral function instead of the one in DDFA when calculating the intrinsic resistivity of metal with the complex Fermi surface.

Before ending our work, we would like to remark briefly on the issue of the potential functional group decoration to MBenes. It is well known that the surface metal atoms of MXenes are easily passivated by certain functional species (e.g., -OH, -F, -O). It is very difficult to get rid of such an effect in MXenes. In contrast, there is no evidence to confirm the existence of functional groups on the experimentally prepared MBenes so far. Li *et al.* [29] have theoretically demonstrated that Ti_2B_2 and Mo_2B_2 have good kinetic stability, mechanical stability, and thermal stability, even free from the decoration of any functional groups. In the near future, accompanying the relevant experimental studies, the theoretical calculations about the electronic and transport properties of MBenes with the decoration of functional groups will be significant. However, in view of the diverse functional groups, to address such a topic implies a huge computa-

tional cost, and which cannot be completely covered by our present work. Herein, as a straightforward reasoning, we can say that if a functional group does not change largely the size and shape of the Fermi surface of MBenes such as the Ti_2B_2 and Mo_2B_2 under our consideration, these materials remain to be good metals due to their very large Fermi surface.

ACKNOWLEDGMENTS

This work was financially supported by the National Natural Science Foundation of China (Grants No. 12174145 and No. 11774123) and the Fundamental Research Funds for the Central Universities. We thank the High Performance Computing Center of Jilin University for providing computing resources.

-
- [1] K. S. Novoselov, A. K. Geim, S. V. Morozov, D. Jiang, Y. Zhang, S. V. Dubonos, I. V. Grigorieva, and A. A. Firsov, Electric field effect in atomically thin carbon films, *Science* **306**, 666 (2004).
- [2] V. G. Nair, M. Birowska, D. Bury, M. Jakubczak, A. Rosenkranz, and A. M. Jastrzębska, 2D MBenes: A novel member in the flatland, *Adv. Mater.* **34**, 2108840 (2022).
- [3] B. Zhang, J. Zhou, and Z. Sun, MBenes: Progress, challenges and future, *J. Mater. Chem. A* **10**, 15865 (2022).
- [4] H. Zhang, H. Xiang, F. Zhi Dai, Z. Zhang, and Y. Zhou, First demonstration of possible two-dimensional MBene CrB derived from MAB phase Cr_2AlB_2 , *J. Mater. Sci. Technol.* **34**, 2022 (2018).
- [5] L. T. Alameda, P. Moradifar, Z. P. Metzger, N. Alem, and R. E. Schaak, Topochemical deintercalation of Al from $MoAlB$: Stepwise etching pathway, layered intergrowth structures, and two-dimensional MBene, *J. Am. Chem. Soc.* **140**, 8833 (2018).
- [6] J. Wang, T.-N. Ye, Y. Gong, J. Wu, N. Miao, T. Tada, and H. Hosono, Discovery of hexagonal ternary phase Ti_2InB_2 and its evolution to layered boride TiB, *Nat. Commun.* **10**, 2284 (2019).
- [7] T. Xu, Y. Wang, Z. Xiong, Y. Wang, Y. Zhou, and X. Li, A rising 2D star: Novel MBenes with excellent performance in energy conversion and storage, *Nano-Micro Lett.* **15**, 6 (2023).
- [8] J. Bardeen and D. Pines, Electron-phonon interaction in metals, *Phys. Rev.* **99**, 1140 (1955).
- [9] J. Ziman, *Electrons and Phonons: The Theory of Transport Phenomena in Solids* (Oxford University Press, UK, 2001).
- [10] P. B. Allen, Fermi-surface harmonics: A general method for nonspherical problems. Application to Boltzmann and Eliashberg equations, *Phys. Rev. B* **13**, 1416 (1976).
- [11] Z. Liu, M. Zhu, and Y. Zheng, Fermi surface nesting and intrinsic resistivity of beryllium: First-principles calculations, *Phys. Rev. B* **100**, 045145 (2019).
- [12] P. Giannozzi, O. Andreussi, T. Brumme, O. Bunau, M. B. Nardelli, M. Calandra, R. Car, C. Cavazzoni, D. Ceresoli, M. Cococcioni, N. Colonna, I. Carnimeo, A. Dal Corso, S. de Gironcoli, P. Delugas, R. A. DiStasio Jr., A. Ferretti, A. Floris, G. Fratesi, G. Fugallo *et al.*, Advanced capabilities for materials modelling with QUANTUM ESPRESSO, *J. Phys.: Condens. Matter* **29**, 465901 (2017).
- [13] N. Troullier and J. L. Martins, Efficient pseudopotentials for plane-wave calculations, *Phys. Rev. B* **43**, 1993 (1991).
- [14] J. P. Perdew, K. Burke, and M. Ernzerhof, Generalized gradient approximation made simple, *Phys. Rev. Lett.* **77**, 3865 (1996).
- [15] F. Li and Q. Tang, First-principles calculations of TiB MBene monolayers for hydrogen evolution, *ACS Appl. Nano Mater.* **2**, 7220 (2019).
- [16] Y. Xiao, Y. Li, Z. Guo, C. Tang, B. Sa, N. Miao, J. Zhou, and Z. Sun, Functionalized Mo_2B_2 MBenes: Promising anchoring and electrocatalysis materials for lithium-sulfur battery, *Appl. Surf. Sci.* **566**, 150634 (2021).
- [17] S. Grimme, Semiempirical GGA-type density functional constructed with a long-range dispersion correction, *J. Comput. Chem.* **27**, 1787 (2006).
- [18] H. J. Monkhorst and J. D. Pack, Special points for Brillouin-zone integrations, *Phys. Rev. B* **13**, 5188 (1976).
- [19] S. Poncé, E. R. Margine, C. Verdi, and F. Giustino, EPW: Electron-phonon coupling, transport and superconducting properties using maximally localized Wannier functions, *Comput. Phys. Commun.* **209**, 116 (2016).
- [20] T. Sohler, M. Calandra, C.-H. Park, N. Bonini, N. Marzari, and F. Mauri, Phonon-limited resistivity of graphene by first-principles calculations: Electron-phonon interactions, strain-induced gauge field, and Boltzmann equation, *Phys. Rev. B* **90**, 125414 (2014).
- [21] B. Zhang, F. Guo, L. Zhang, M. Zhu, and Y. Zheng, Controllable sign reversal of Seebeck coefficient and the large tunability of ZT value of plumbene: A first-principles study, *J. Mater. Chem. C* **9**, 16645 (2021).
- [22] A. D. Dillon, M. J. Ghidui, A. L. Krick, J. Griggs, S. J. May, Y. Gogotsi, M. W. Barsoum, and A. T. Fafarman, Highly conductive optical quality solution-processed films of 2D titanium carbide, *Adv. Funct. Mater.* **26**, 4162 (2016).
- [23] B. Zhang, M. Zhu, Z. Liu, F. Guo, and Y. Zheng, Temperature-dependent electron-phonon spectral function and the intrinsic resistivity of a metal: A case study of monolayer Ti_2N , *Phys. Rev. B* **102**, 165402 (2020).
- [24] M. Naguib, O. Mashtalir, J. Carle, V. Presser, J. Lu, L. Hultman, Y. Gogotsi, and M. W. Barsoum, Two-dimensional transition metal carbides, *ACS Nano* **6**, 1322 (2012).

- [25] M. Ghidui, M. Naguib, C. Shi, O. Mashtalir, L. M. Pan, B. Zhang, J. Yang, Y. Gogotsi, S. J. L. Billinge, and M. W. Barsoum, Synthesis and characterization of two-dimensional Nb₄C₃ (MXene), *Chem. Commun.* **50**, 9517 (2014).
- [26] Z. Liu, M. F. Zhu, and Y. S. Zheng, First-principles calculations on the intrinsic resistivity of borophene: Anisotropy and temperature dependence, *J. Mater. Chem. C* **7**, 986 (2019).
- [27] W. E. Lawrence and J. W. Wilkins, Umklapp electron-phonon scattering in the low-temperature resistivity of polyvalent metals, *Phys. Rev. B* **6**, 4466 (1972).
- [28] P. N. Trofimenkoff and J. W. Ekin, Electron-phonon umklapp scattering processes in the low-temperature ultrasonic attenuation and electrical resistivity of potassium, *Phys. Rev. B* **4**, 2392 (1971).
- [29] X. Zhu, X. Zhou, Y. Jing, and Y. Li, Electrochemical synthesis of urea on MBenes, *Nat. Commun.* **12**, 4080 (2021).